Mechanical Properties of Polyurethane-Stabilized Ballast

A. Keene[1], J.M. Tinjum[2] and T.B. Edil[3]
[1]*Graduate Research Assistant, Dept. of Civil, Architectural, and Environmental Engineering, University of Texas at Austin, USA*
[2]*Assistant Professor, Dept. of Engineering Professional Development, University of Wisconsin-Madison, Madison, USA*
[3]*Professor Emeritus and Director, Recycled Materials Resource Center and Wisconsin Highway Research Program, University of Wisconsin-Madison, Madison, USA*
[1]*E-mail: akkeene@utexas.edu*
[2]*E-mail: jmtinjum@wisc.edu*
[3]*E-mail: tbedil@wisc.edu*

ABSTRACT: Ever increasing volume, tonnage, and speeds on rail systems are stressing rail substructure to levels never before evaluated or considered in depth. To improve maintenance techniques for problematic railway elements (e.g., bolted rail joints, intersections, bridge approaches), an *in situ* method involving ballast layer reinforcement with polyurethane is proposed. Ballast is a crucial material for structural support of the rail tracks. The structural integrity of highly fouled ballast (i.e., containing fine particles) can be compromised leading to track instability and ultimately train derailments. An application using polyurethane void filling and particle bonding technology has been developed and has the potential to mitigate impacts of ballast fouling, enhance rail freight capacity, and improve track-substructure maintenance efficiency. The purpose of this paper is to present the mechanical properties of Polyurethane-Stabilized Ballast (PSB) (e.g., compressive and flexural response), compare these properties to other materials commonly used in transportation infrastructure (e.g., natural aggregates, cement-stabilized soil), and address the suitability and compliance of PSB for use in track infrastructure. PSB has mechanical properties similar to cement-stabilized soil (i.e., displays flexural strength), but has much greater compressive strength than ballast, which is critical for stabilization of track substructure. Ease of injection and the negligible curing period for PSB makes it an attractive option for railway maintenance, especially for time-sensitive maintenance activities, such as intersections and bridge approaches.

1. INTRODUCTION

Rigid-polyurethane foam (RPF) applied to granular materials, after injection and solidification, improves the strength by occupying the pore space and cementing the particles together. Due to the expansive properties of the foam, it has historically been applied in foundation engineering to support footings and slabs. Due to these advantages, there have been efforts to expand the applicability of RPF to other infrastructure settings, including the rail industry. The necessity for reinforcing railway substructure with strategic RPF injections include: 1) reducing particle breakage and fines intrusion, thus mitigating fouling generation, 2) correcting already fouled ballast substructure and arresting permanent deformation in the track, 3) improving substructure performance and preserving track geometry thereby enhancing rail-freight capacity and rider-comfort, and 4) providing a cost- and time-effective maintenance tool to supplement rail maintenance capabilities.

For a railway embankment, the superstructure (i.e., rails, ties, and fastening system) serves as a rigid structure that distributes the loads over a large surface area to the substructure (i.e., ballast, subballast, and subgrade) (Huang 2004). The superstructure typically has much longer lifecycle than the substructure; however, the superstructure lifecycle is dependent upon substructure conditions and substructure maintenance intervals (Ebrahimi et al. 2012). Therefore, when considering polyurethane-stabilized ballast (PSB) for use in constructing a stabilized substructure, the mechanical behavior relative to other materials used in transportation infrastructure needs to be evaluated.

Polyurethane interacts differently with the injected medium depending on the nature of the medium. For instance, Buzzi et al. (2012) injected RPF into expansive clay and found that the injection created hydrofractures while forming into dendritic paths of foam. Keene (2012) injected RPF into rail ballast (which has a more favorable void structure for RPF injection) and formed a solid, uniform geocomposite. The pore space in compacted ballast conveniently allows injection of polyurethane, allowing space for RPF expansion, and for target RPF volumes and densities to be met. Keene (2012) proposed a set of criteria by which the mechanical properties of the ballast layer were improved with polyurethane injections. These criteria include: 1) extent to which the void space of ballast was filled by the RPF, 2) strength and degree of bonding that occurred between the ballast particles and RPF, and 3) limiting volumetric expansion of ballast during RPF injection. Many methods are available for the mechanical analysis of polymeric cellular foams or for engineering properties of granular materials; however, little is understood about the behavior of the combination of an expanding polymer with ballast and effects on the mechanical properties within track-substructure.

The objective during field injection of RPF into the ballast layer is to strengthen the areas that transmit load down into the subballast and subgrade layers. Moisture is prevented from infiltrating the stabilized areas while drainage of surrounding untreated ballast is left uninhibited. Ballast layer prototypes (i.e., boxes filled with 0.45-m-deep compacted ballast) were also created in Keene (2012), where RPF was strategically injected into an unconfined layer of ballast. In that physical model, methods for targeting the dimensions of the stabilized areas were developed.

In this paper, specimen fabrication and experimental methods for compressive and flexural testing and analysis of polyurethane-stabilized ballast (PSB) are presented. Moduli and strength of each of the constituents of PSB (i.e., ballast and RPF) are compared to each other and to the PSB composite material. The mechanical properties of PSB and PSB constituents (RFP and ballast) are compared to other materials such as cement-stabilized materials (CSM), natural base-course aggregates, and concrete for a broader perspective. Compressive and flexural strength of PSB and RPF are compared to CSM (at different cement-binder contents) to show the similarity in relative strengths of these materials. Resilient modulus of PSB, ballast, MN DOT Class 5 aggregate, and CSM are compared to show the elastic behavior of the materials under cyclic loading conditions. Flexural strength of CSM and PSB are compared to demonstrate increase in strength with increase in binder content (i.e., percent cement and percent RPF by weight). The strength-to-bulk-density ratio (σ/ρ) of PSB, RPF, ballast, CSM, and concrete are compared to show how each material possesses σ/ρ properties that can be favorable depending on the application. The purpose of this

study was to measure the mechanical properties of PSB, relate these properties to properties of other materials commonly used in transportation infrastructure, and to evaluate the suitability of PSB for use in track infrastructure.

2. MATERIALS

Ballast (Figure 1) was provided by BNSF Railway Company from a quarry near Cheyenne, Wyoming. The particle size distribution ranged between 25 and 63 mm (ASTM D6913). Maximum dry unit weight was obtained following the procedure developed in Ebrahimi et al. (2012), resulting in a clean ballast void ratio, e_b, of 0.62. The corresponding clean ballast dry unit weight (γ_d) and density (ρ_d) were 15.8 kN/m^3 and 1,611 kg/m^3, respectively. These compaction characteristics were targeted in fabrication of each specimen of clean ballast injected with RPF in this study.

For characterizing fouled ballast, two conventions commonly used are fouling index (FI) and moisture content (MC) (Selig and Waters 1994, Ebrahimi et al. 2012). The fouling index comprises of adding percent of particles passing through a 4.75-mm (P4) sieve and percent of particles passing a 0.075-mm (P200) sieve. Ballast with FI between 20% and 39% is considered highly fouled.

The 486STAR-4 BD, a RPF supplied by Uretek USA Inc., is a two-component, high-density, expanding, thermoset, polyurethane-resin system. The 486STAR-4 BD (Figure 1) was formulated by Bayer Material Science in partnership with Uretek USA Inc., for different applications including void filling and sealing. For synthesis of thermoset polyurethane-resin foams, the two components (polyester or polyether polyol and organic polyisocyanate) are proportionately mixed in the presence of a catalyst (Szycher, M. 1999). The foam structure results from gas bubble formation during the polyurethane polymerization process, known as *blowing*. Gas bubble formation is the result of introducing the *blowing agent* (Szycher, M. 1999). As detailed in Keene (2012), the cellular structure of the RPF is an important component for providing RPF strength and modulus. The greater the extent of the closed-cell structure (ASTM D6226) the greater the strength and modulus of RPF. In the technical data sheet produced by Bayer Material Science (2010), the 486STAR-4 BD is indicated to possess a closed-cell content of 90%.

During injection, RPF flows as a liquid and expands through the ballast pore space. While the RPF transitions through the polymer curing phases, bonds are established with materials in contact with the reacting RPF. When the reaction is completed, a bonded geocomposite is formed and referred herein as polyurethane-stabilized ballast (PSB -Figure 1). The average resulting RPF phase densities within the PSB composite specimens were 200 kg/m^3, further details regarding phase calculations and typical PSB constituent densities are given in Keene (2012). The bonding of RPF with the ballast particles is a critical interaction that takes place during the polyurethane foaming process. The bonding is attributed to rough surfaces of the ballast particles and intermolecular bonds formed during the polyurethane reaction with the aggregate mineralogy (Keene 2012), which are common characteristics that control strength in asphalt and concrete. Application of PSB formation is an *in situ* stabilization method that does not require premixing with aggregates, soil, or with water, would not require track shutdown, and reaches 90% of full strength within 15 min of application.

3. METHODS

3.1 Flexural Loading of PSB Beams

A method for testing PSB beam specimens was developed from standards for testing concrete and soil-cement beams for flexural strength and fatigue analysis. The method used for determining flexural strength was adopted from ASTM C78 and ASTM D1635 and the method used for ascertaining flexural fatigue properties was adopted from an AUSROADS procedure described in Midgley and Yeo (2008). The two methods are commonly used for determining flexural strength and fatigue characteristics of materials for use in transportation infrastructure because of the cyclic loading that occurs. From these procedures and standards, a "third-point" loading setup was selected. A "third-point" loading setup is ideal for reducing the effects of shear stress during flexural testing and for an improved analysis of flexural strength and fatigue properties. The dimensions of the beams from previous standards (e.g., ASTM D1635) were increased by a ratio of 2.63:1 to account for the large particle sizes in ballast. The dimensions used for the PSB beam molds were 200 mm x 200 mm x 763 mm. Further detail on beam specimen fabrication, flexural testing procedures, methodology, and data analysis are given in Keene (2012).

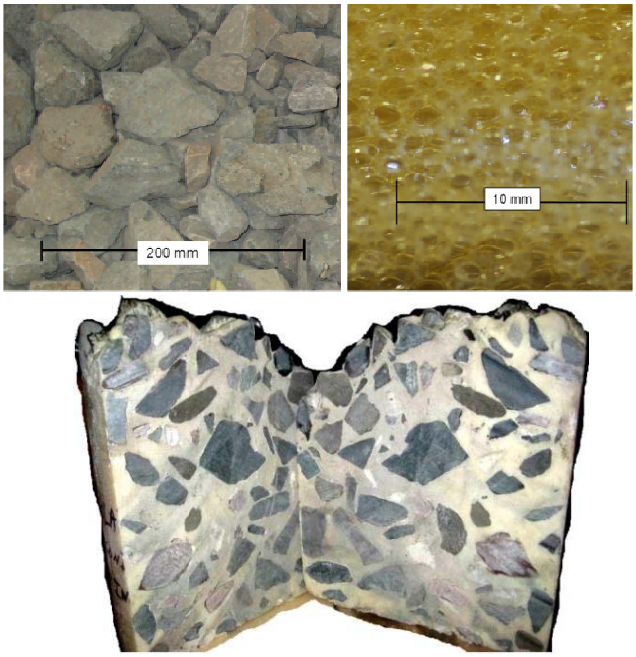

Figure 1 Pictures of granitic ballast (top-left), RPF foam (top-right), and PSB specimen cut in half with concrete masonry saw (bottom)

In the flexural beam tests, the load is applied to a fixture that distributes the load evenly through two loading rollers at the two upper-inner "third-points" of the beam. Rollers on the two lower-outer "third-points" of the beam support the beam. The flexural strength (kPa), otherwise known as rupture modulus (R), is calculated as

$$R = \frac{P \cdot L}{w \cdot h^3} \qquad (1)$$

where P is the peak load (kN) during the test or load before rupture, L is the span length (m) between the bottom supports of the setup, w is the base width (m) of the beam, and h is the depth (m) or dimension of the beam between the top and bottom supports, all of which are shown in Figure 2.

The flexural modulus is derived using elastic beam theory where flexural stress and strain are inferred from applied loads and corresponding deflection at the mid-span of the beam. In Midgley and Yeo (2008) and this study, the beam flexural modulus, flexural strain, and flexural stress were calculated using elastic beam theory as

$$S_{max} = \frac{\sigma_t}{\varepsilon_t} \cdot 10^3 = \frac{\frac{P \cdot L}{w \cdot h^2} \cdot 10^3}{\frac{108 \cdot \delta \cdot h}{23 \cdot L^2} 10^3} = \frac{23 \cdot P \cdot L^3}{108 \cdot w \cdot h^2 \cdot \delta} \qquad (2)$$

where S_{max} is the flexural modulus (MPa), σ_t is the flexural stress (kPa), ε_t is the flexural strain (m/m), P is the peak load (kN), w is the width of the beam (m), h is the height of the beam (m), L is the span

(m) between bottom two supports of the "third-point" loading setup, and δ is the deflection (m) at the mid-span under the corresponding load.

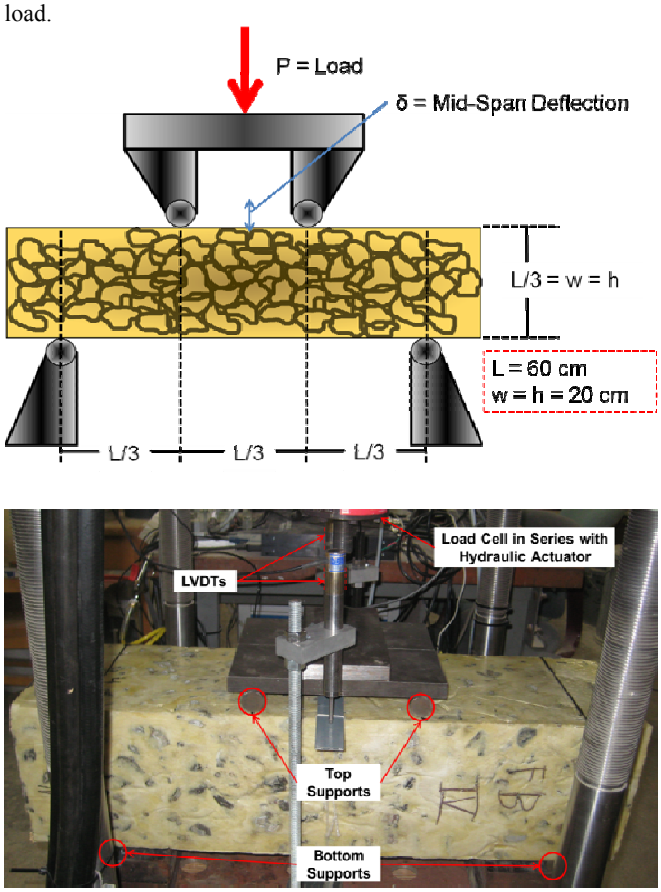

Figure 1 Typical "third-point" loading setup and chosen dimensions for PSB beams

3.2 Unconfined Compressive Strength (UCS) Testing of PSB Prisms

Prismatic specimens with a 2:1 (height-to-width) ratio were created for unconfined-compression strength (UCS) testing. Nominal PSB prism dimensions were 200 mm x 200 mm x 400 mm. The PSB prisms were subjected to UCS tests, which involved placement in a loading machine that compressed the specimens while measuring load and displacement. Further detail on prism specimen fabrication, UCS testing procedures, methodology, and data analysis are covered in Keene (2012).

Unconfined compressive strength (σ_c) was determined by

$$\sigma_c = \frac{F}{A} \tag{3}$$

where F is peak axial load (kN) applied and A is the area (m^2) over which it is applied, both are diagramed in Figure 3. A typical phenomenon in elastic-plastic material is that initially elastic strain (ε_e) increases linearly with axial stress until reaching the yield point, where plastic strain (ε_e) increases and the relationship to stress is no longer linear.

Young's modulus, E, occurs within the linear region and is defined by

$$E = \frac{\sigma}{\varepsilon_e} \tag{4}$$

where σ is the axial stress (kPa) being applied within the elastic range of the material.

3.3 Cyclic Triaxial Compression Testing of PSB Cylinders

Cylindrical specimens with a minimum diameter of 254 mm provides an appropriate particle diameter to specimen diameter ratio similar to the one used in the study by Anderson and Fair (2008) on triaxial testing of railway ballast. Clean ballast specimens were tested in a triaxial cell and the corresponding results were validated with the data given in Ebrahimi et al. (2012). Further details on cylindrical specimen fabrication, cyclic-triaxial compression testing procedures, and data analysis are given in Keene (2012)

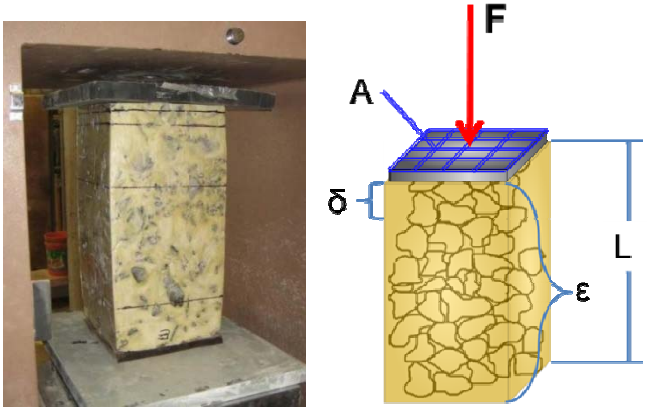

Figure 2 Picture of compression testing apparatus (left) and diagram of compression testing parameters (right)

The cyclic triaxial compression test consists of applying a constant confining pressure (σ_3) to a specimen that is contained within a membrane and sealed in a triaxial chamber. A plunger or piston that extends through a seal in the top plate of the triaxial cell applies the cyclic load. The cyclic load is applied as a 5-Hz haversine, bell-shaped loading pulse with peak and rest loads (Ebrahimi et al. 2012). The deviator stress at peak (300 kPa) and during the rest (17.6 kPa) period is given by

$$\sigma_p = \sigma_r = \frac{F}{A} \tag{5}$$

where the load (F) from the piston (kN) is applied through the area (A) of the plate on top of the specimen (m^2). After each loading cycle, non-recoverable deformation (plastic deformation, δ_P) is measured and recoverable deformation (elastic deformation, δ_E) is found by subtracting δ_P from the measured total deformation (δ_T) in each load pulse, and the elastic strain ε_E is calculated as

$$\varepsilon_E = \frac{\delta_E}{L} \tag{6}$$

where L is specimen length.

The resilient modulus is denoted as M_R (kPa) and is calculated from

$$M_R = \frac{\sigma_P - \sigma_R}{\varepsilon_E} \tag{7}$$

where σ_P is peak stress (kPa), σ_R is rest stress (kPa), and ε_E is elastic strain (m/m).

The resilient modulus is cyclic Young's modulus and quantifies the stiffness of a material. In the cyclic triaxial tests, the calculation of the resilient modulus over many loading cycles reveals how the stiffness changes over the life cycle of the material or reaches a constant value after numerous loading cycles. In either case, M_R provides the operational resilient properties of a material. Additionally, accumulated plastic strains (ε_p) with number of loading cycles are also recorded in this test.

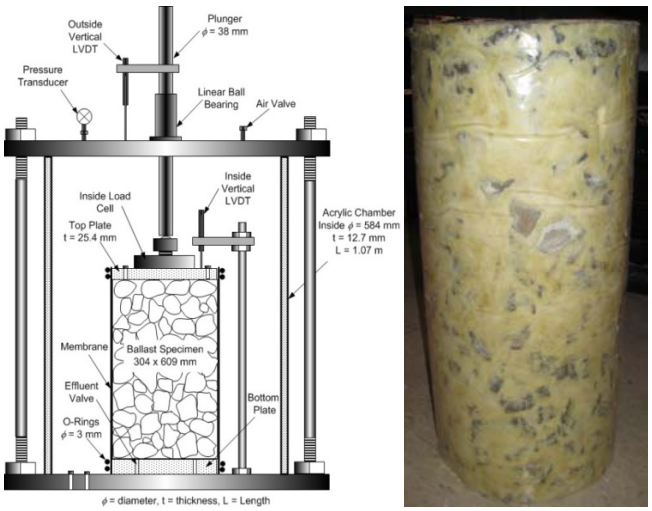

Figure 4 Triaxial chamber used for testing specimens with nominal dimensions of 254-mm diameter x 506-mm height (left) and PSB cylindrical specimen (right)

4. RESULTS

4.1 Mechanical Properties of PSB and Infrastructure Materials

4.1.1 Mechanical Properties of PSB Constituents

RPF strengths are similar in each mode of testing, as seen in Figure 5. When comparing flexural test results, when the average (AVG) RPF density, ρ_{RPF}, is 200 kg/m^3, the AVG PSB flexural modulus (274 MPa) is greater than the AVG RPF flexural modulus (124 MPa); however, the AVG PSB flexural strength of 938 kPa is less than the AVG RPF flexural strength 3,652 kPa as shown in Figure 5. Greater flexural stiffness of PSB compared to RPF can be attributed to the stiffness of the ballast particles. The lower flexural strength of PSB relative to RPF can be attributed to weakness in the bonding interface between the ballast particles and RPF. As described in Akçaoğlu et al. (2003), the surface texture and the bonding area between cement binder and aggregates are critical to concrete strength and stiffness. Akçaoğlu et al. (2003) defined this bonding area as the interfacial transition zone (ITZ) and described this zone as the weakest component in concrete mechanical behavior. When focusing on an ITZ for PSB, the strength of the composite can be attributed to two likely factors: 1) RPF-ballast bond interface strength and 2) PSB composite/matrix strength based on cell orientation/geometry within the ballast pore space and around ballast particles. The flexural strength and tensile strength of RPF are greater than the flexural strength of PSB; consequently, the ITZ for PSB likely controls flexural strength. The cellular structure of RPF (as characterized by closed-cell content, cell-wall thickness, cell elongation, and cell aperture) likely plays a large role in RPF strength and elastic modulus.

In Salim (2004), the compressive strength of ballast particles was used for determining the characteristic tensile strength of the ballast. Salim (2004) cites Jaeger (1967) for explaining that the fracture of rock grains occurs due to tensile failure and that fracture strength in tension can be measured indirectly through compression tests conducted on rock particles using "diametral compression between flat platens." Trends establishing RPF tensile strength versus density (Keene 2012) indicate that at a characteristic RPF density of 200 kg/m^3, the corresponding tensile strength is 3,912 kPa, which is far less than the characteristic particle tensile strength (5,400 kPa to 22,300 kPa) of the granite ballast used in this study as reported by Ebrahimi et al. (2012). Since the characteristic tensile strength of ballast is higher than the tensile strength of RPF, RPF may govern the rupture strength of PSB in monotonic flexural loading tests. However, failure likely occurs at the ITZ since the AVG PSB flexural microstrain (με) at rupture (8.94 με) is less than RPF (ρ_{RPF} = 200 kg/m^3) flexural microstrain at rupture (28.7 με).

Characteristic tensile strength of ballast particles is the only instance where ballast would contribute to the overall strength of PSB instead of RPF. Higher tensile strength of ballast particles (i.e., higher stiffness) must also contribute to the flexural stiffness of PSB being higher than the compressive stiffness of PSB. However, it is likely that in fatigue testing conducted in Keene (2012), fatigue of ballast particles contributed to fatigue failure since fracture of ballast particles was observed after the fatigue testing. Therefore, ballast particles may fatigue under flexural/tensile loading before RPF fatigue occurs.

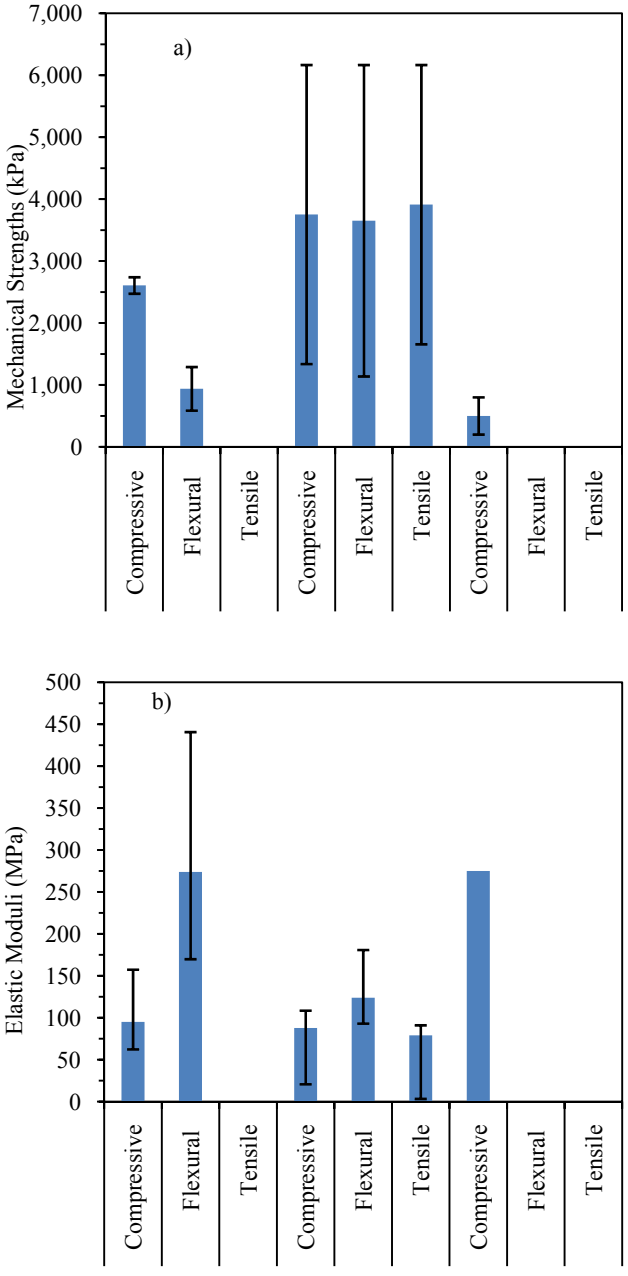

Figure 5 Shown are the mechanical strengths (a) and moduli (b) for PSB and PSB constituent materials. Representative mechanical properties of RPF are at a 200 kg/m^3-density. Representative ballast compressive modulus and strength are at a 100-kPa confining stress (Ebrahimi et al. 2012). Error bars indicate maximum and minimum mechanical property values (i.e., range) for materials with varying confining stresses (ballast) or densities (RPF and PSB).

Similar to the PSB constituent flexural strengths, the RPF (ρ_{RPF} = 200 kg/m^3) compressive strength (3,752 kPa) is higher than the AVG PSB compressive strength (2,607 kPa). Ballast compressive strength at 100 kPa confining pressure is 594 kPa, which is 77% less than PSB. A limitation in PSB compressive strength relative to RPF compressive strength is likely due to limits in bonding strength (i.e., weakness of the ITZ), as was identified for PSB flexural strength. However, an increase in PSB compressive strength relative to ballast compressive strength is attributed to both the predominant strength of RPF and the high characteristic ballast tensile strength. Similar interactions take place with aggregates and asphalt binder resulting in the superior behavior of asphalt mixes (Tia 2003).

Marginal differences were observed between PSB compressive modulus (95 MPa) in monotonic loading tests and resilient modulus (100 MPa) in cyclic triaxial tests. Therefore, monotonic testing on PSB can be a useful alternative for predicting PSB resilient modulus generally determined under cyclic compressive loading. Regarding deformational behavior of PSB, minimal accumulation of plastic strain, ε_p, was observed over 200,000 loading repetitions at a representative state of stress (Ebrahimi et al. 2012) in PSB cylinders in cyclic triaxial testing. Specimens tested up to 500,000 loading repetitions had a marginal increase in plastic strain. Over the first 200,000 loading repetitions, PSB plastic strain (ε_p = 0.22%) was far less than clean ballast (ε_p = 0.96%) or fouled ballast (ε_p = 3%) with a fouling index of 5% and moisture content of 15%. Cumulative plastic strain is the main limiting performance parameter for clean or fouled ballast. However, the cumulative plastic strain under cyclic loading conditions in PSB specimens was significantly reduced making PSB elastic properties a more important performance parameter for design of PSB in rail substructure. Since PSB and RPF compressive strengths are far greater than the clean ballast compressive strength (at the representative confining stress), the functionality of PSB in rail infrastructure would likely be driven by PSB compressive modulus.

4.1.2 PSB Mechanical Properties Compared to Bounded and Unbounded Aggregates

When comparing the compressive strength of PSB to cement-stabilized materials (CSM), PSB has 2.5 times less compressive strength (see Figure 6). RPF with a 200-kg/m^3 density has a compressive strength of 3,752 kPa and ballast (tested at 100 kPa confining pressure) has a compressive strength of 594 kPa; therefore, both materials possess lower compressive strengths than CSM. From RPF test results compiled from literature (Keene 2012), RPF with a density ranging from 26 to 417 kg/m^3 has compressive strength ranging from 2,774 kPa to 6,167 kPa (Figure 6); therefore, CSM still possesses higher strength than RPF formed at high densities.

When comparing the flexural strength of PSB and RPF to CSM, as shown in Figure 6, PSB has a flexural strength similar to that of CSM flexural strength tested at 28-day curing time given by Midgley and Yeo (2008). RPF (ρ_{RPF} = 200 kg/m^3) possesses a much higher flexural strength (3,652 kPa) than PSB and CSM. With RPF density ranging from 26 to 417 kg/m^3, the range of RPF flexural strength is 2,774 kPa to 6,167 kPa, which is greater than both PSB and CSM (Figure 6). In Midgley and Yeo (2008), the flexural modulus increased as the relative density increased, similar to how modulus of PSB increases as PSB density increases (Keene 2012). Unlike the materials being compared to RPF, RPF has similar strengths in each mode of load application (i.e., compressive, flexural, and tensile) and, as indicated later in this paper, RPF has superior strength-to-bulk-density ratio.

Since PSB and CSM have similar AVG flexural strength properties, a comparison is also made between flexural strength and the percentage of binder content. A study by Zhang and Wei (2011) is used for comparison where the flexural strength of CSM (at 28-day curing time) was marginally higher than CSM strength given in Midgley and Yeo (2008) that was used in earlier comparisons. With a range of binder content (percent cement) from 4 to 7%, the flexural strength of CSM reported in Zhang and Wei (2011) ranged from 1,150 kPa to 1,895 kPa, corresponding to a 39% increase in flexural strength with 3% increase in binder content. Over the same range of binder content in PSB (percent RPF by weight), PSB flexural strength ranged from approximately 682 kPa to 1,290 kPa, corresponding to a 28% increase. PSB and CSM flexural strength versus binder contents are shown in Figure 7. Thus, an increase in cement binder content is more effective in increasing the flexural strength of CSM in comparison to an increase in RPF binder content on the flexural strength increase in PSB. In addition, an increase in volume of RPF in PSB is much higher than an increase in volume of cement needed to obtain the same proportional increase in flexural strength.

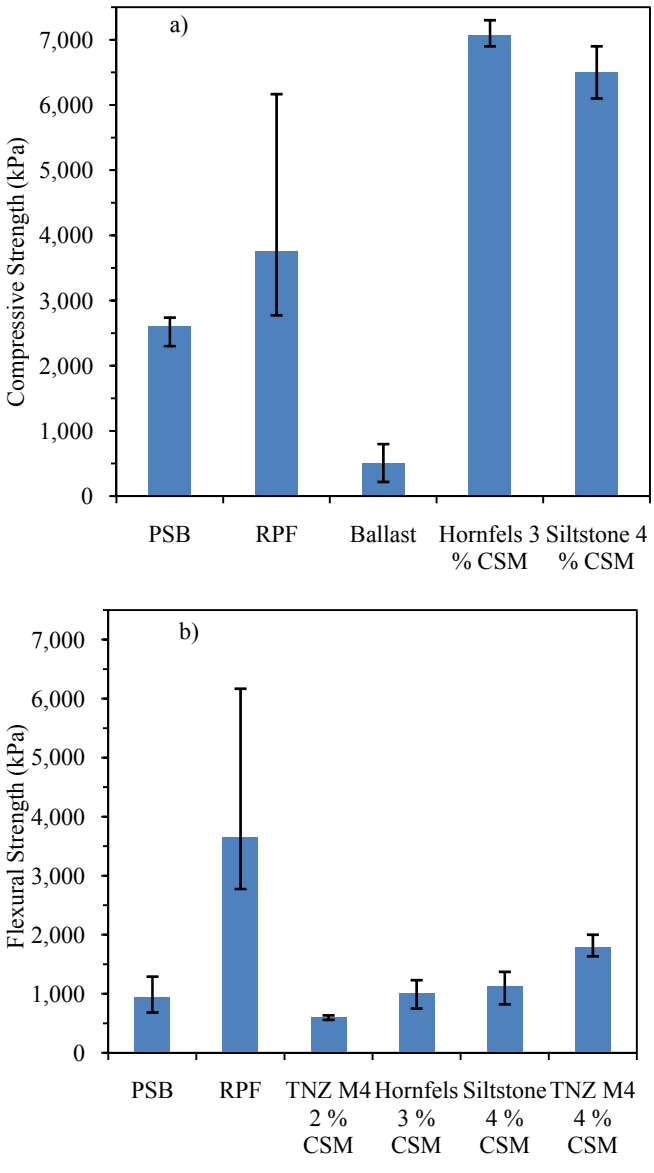

Figure 6 Comparison of RPF and CSM compressive strengths (a) and comparison of RPF and CSM flexural strengths (b). Hornfels and Siltstone data are from Midgley and Yeo (2008) and TNZ M4 are from Arnold (2009).

The flexural strength of RPF is greater compared with other materials (e.g., CSM and PSB); however, CSM has greater compressive strength than PSB or RPF at a density of 200 kg/m^3. In addition, CSM has far greater flexural modulus (AVG 13,800 MPa)

than PSB and RPF (274 and 124 MPa, respectively). Consequently, CSM would perform more favorably in applications where minimal compliance (i.e., elastic strain) is allowed under operational flexural loading conditions, hence the typical application of CSM in roadway construction. For rail infrastructure, higher compliance of PSB may be favorable due to the strains that can be tolerated under the loads distributed from the superstructure down through the substructure.

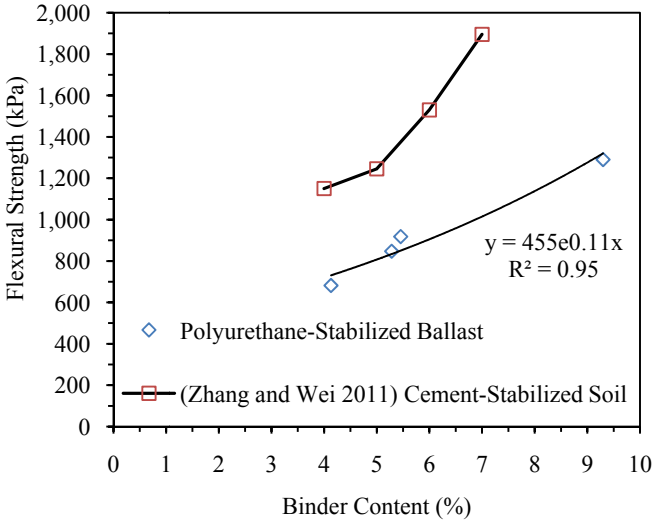

Figure 7 Comparison of PSB and CSM flexural strength versus binder content (percent RPF and percent cerement, respectively)

When evaluating the M_R of PSB, ballast, MN DOT Class 5 aggregate, and CSM (Figure 8); PSB (AVG 100 MPa) has the lowest M_R, while CSM with 2% cement binder tested by Arnold (2009), has the highest modulus. MN DOT Class 5 tested at a bulk stress of 208 kPa had a M_R that was 18% less than ballast and over 2 times greater than PSB. The M_R of ballast (275 MPa) was over 2.5 times greater than PSB. When PSB density ranged 1,536 to 1,683 kg/m^3, M_R ranged 63–181 MPa, which is still less than the M_R of ballast. As is the case for flexural properties of CSM, CSM would perform more favorably in applications where higher stiffness is required for design under compressive loading. A finite element analysis determined that the effect on the overall elastic response of the track was inconsequential when PSB with a lower compressive modulus was included in the track substructure (Keene et al. 2013).

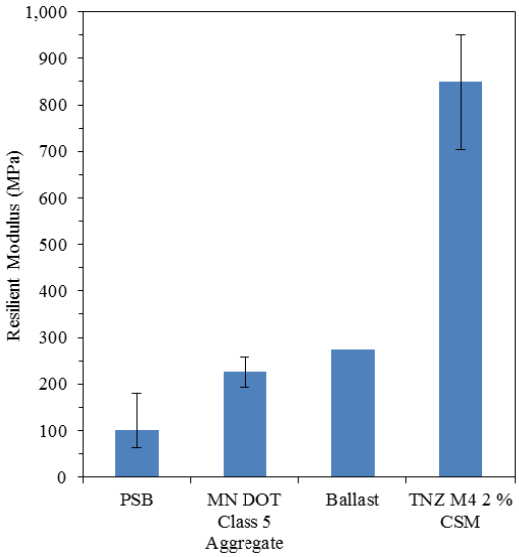

Figure 8 Comparison of resilient modulus of PSB, clean ballast at bulk stress of 600 kPa (Ebrahimi et al. 2012), summary resilient modulus of MN DOT Class 5 tested at a bulk stress of 208 kPa, and CSM with 2% cement binder tested by Arnold (2009).

The compressive properties of PSB, RPF, and ballast are compared using average strength-to-bulk-density ratio (σ/ρ, kPa/kg/m^3) in compression to show how the strength compares to the density or weight of the materials (Figure 9). RPF (σ/ρ = 18.8) has a σ/ρ far greater than that of ballast (σ/ρ = 0.31) tested at 100 kPa confining stress. The mechanical properties of PSB and RPF are also compared using average flexural σ/ρ to show how the strength compares to the weight of the materials under flexural loading conditions (Figure 9). As was seen for compressive σ/ρ, RPF (σ/ρ = 18.3) has the highest flexural σ/ρ of the materials. For comparison, PSB has a flexural σ/ρ of 0.57, CSM with 4% cement, from Midgley and Yeo (2008) (AVG bulk density of 2,146 kg/m^3) has a σ/ρ of 0.53, and concrete (2,403-kg/m^3 bulk density) designed for 20.7 GPa compressive strength has a flexural σ/ρ of 1.31. When comparing flexural σ/ρ, RPF has the same ratio in compression as in flexure. As was seen with flexural strength properties of PSB and CSM, both materials have a very similar flexural σ/ρ, with CSM having a marginally lower σ/ρ than PSB.

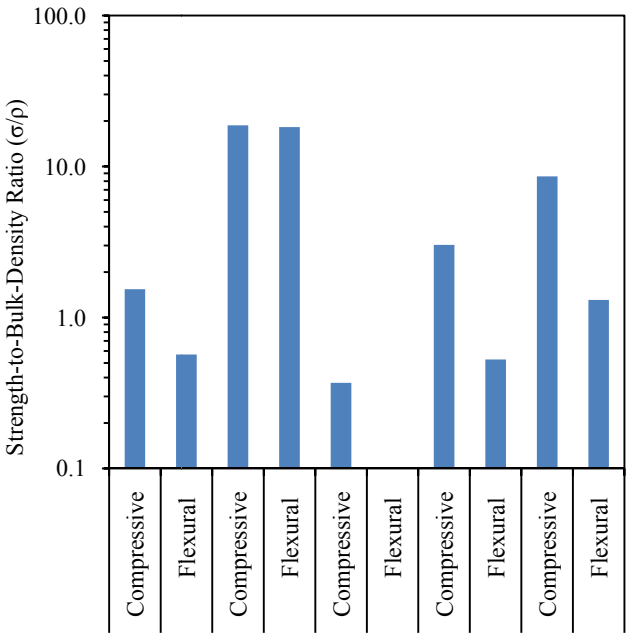

Figure 9 Comparison of the strength-to-bulk-density ratio (log-scale) of PSB constituents, PSB, typical 20.7 GPa concrete, and 4% cement siltstone from Midgley and Yeo (2008). Log-scale used so that each ratio can be visualized in the figure.

5. CONCLUSIONS

In this study, the mechanical properties of polyurethane-stabilized ballast (PSB) are compared to that of its constituent parts and other materials typically used in transportation infrastructure. The compressive strength of PSB is much greater than clean ballast, but less than CSM. The flexural strength of PSB is very similar to CSM, with PSB stiffness being a little lower. The resilient modulus of PSB is lower than clean ballast, CSM, and typical highway base-course aggregate; however, contribution of the lower PSB stiffness to track deformational response is not considered to be significant and perhaps may be beneficial. Most significantly, the accumulation of PSB plastic strains under cyclic loading is far less than clean and fouled ballast.

Based on the mechanical properties of PSB presented herein, PSB has at least two potential applications. First, when stabilizing ballast from the bearing surface of the tie down to the subballast layer, the compressive strength results and resistance to accumulation of plastic strain indicate that these areas can have much longer life cycle than untreated ballast. Second, when

stabilizing ballast at the base of the ballast layer (i.e., as an underlayment), the flexural strength results indicate that PSB can withstand loading while serving to prevent intrusion of fines and water from the subballast and subgrade layers. Data and performance from actual field installation of PSB is still needed for validating the laboratory results.

PSB is found to have suitable mechanical properties for use as a material in track-substructure. The ease of injections and negligible curing period for implementation of PSB makes it an attractive alternative for railway maintenance. PSB may find appropriate application in areas that cannot afford track shutdown or where traditional maintenance capabilities are impeded or unachievable.

6. ACKNOWLEDGEMENTS

This research was funded by the National Center for Freight and Infrastructure Research and Education. The contents of this report reflect the views of the authors, who are responsible for the facts and the accuracy of the information presented herein. The U.S. Government assumes no liability for the contents or use thereof. The contents do not necessarily reflect the official views of the National Center for Freight and Infrastructure Research and Education, the University of Wisconsin, the Wisconsin Department of Transportation, or the USDOT's RITA at the time of publication. Contributions of Mr. Steven Reed and Dr. Randall Brown of Uretek USA, Mr. Henry Lees of BNSF Railway Company, Dr. Ali Ebrahimi of Geosyntec, Inc., and Ben Warren of the University of Wisconsin-Madison are gratefully acknowledged.

7. REFERENCES

Akçaoğlu, T., Mustafa, T., and Çelik, T. (2003). "Effect of Course Aggregate Size and Matrix Quality on ITZ and Failure Behaviour of Concrete Under Uniaxial Compression." Cement & Concrete Composites, 26, 633–638. Elsevier Ltd.

Anderson, W.F. & Fair, P. (2008). "Behavior of Railroad Ballast under Monotonic and Cyclic Loading." Journal of Geotechnical and Geoenvironmental Engineering, ASCE, 134(3), 316–328.

Arnold, G. (2009). "Reducing the risk of pavement failure and utilisation of local materials in New Zealand through Repeated Load Triaxial and Beam Fatigue Tests." AAPA Thirteenth International Flexible Pavements Conference, Gold Coast, Queensland, Australia, October 11-13, 2009.

Bayer Material Science. (2010). 486STAR Polyurethane Foam Grout. Technical Data Sheet, Spring, Texas.

Buzzi, O., Fityus, S., & Sloan, S. (2010). "Use of Expanding Polyurethane Resin to Remediate Expansive Soil Formations." Canadian Geotechnical Journal, 47, 623–634.

Ebrahimi, A., Tinjum, J. M. and Edil, T. B. (2012) "Protocol for Testing Fouled Railway Ballast in Large-Scale Cyclic Triaxial Equipment," Geotechnical Testing Journal, ASTM, Vol. 35, No. 5, pp. 796-804.

Huang, Y.H. (2004). Pavement analysis and design – second addition. Pearson Prentice Hall, Upper Saddle River, NJ.

Jaeger, J.C. (1967). "Failure of Rocks Under Tensile Conditions." International Journal of Rock Mineral Science, 4, 219–227.

Keene, A.K. (2012). "Mitigating ballast fouling and enhancing rail-freight capacity." Master's thesis, Department of Civil and Environmental Engineering, University of Wisconsin–Madison.

Keene, A., Edil, T.B., Fratta, D., and Tinjum, J.M. 2013. "Modeling Effect of Polyurethane Stabilization on Track Response." ASCE Geotechnical Special Publication No. 231, *Proceedings Geo-Congress 2013*, San Diego, CA.

Midgley, L. & Yeo, R. (2008). The Development and Evaluation of Protocols for the Laboratory Characterisation of Cemented Materials. Austroads Publication No. AP–T101/08. Austroads Ltd. Sydney, Australia.

Salim, W.M. (2004). "Deformation and Degradation Aspects of Ballast and Constitutive Modeling Under Cyclic Loading." PhD thesis, School of Civil, Mining, and Environmental Engineering, University of Wollongong.

Selig, E.T. & Waters, J.M. (1994). *Track Geotechnology and Substructure Management*. Thomas Telford, New York, NY.

Szycher, M. (1999). Szycher's Handbook of Polyurethanes. CRC Press, Boca Raton, FL.

Tia, M. (2003). *Bituminous Materials and Mixtures Civil Engineering Handbook, Second Edition.* CRC Press, Inc., Boca Raton, Florida, 45.1-45.36.

Zhang, P., & Wei, X. (2011). "Study on Flexural Strength and Flexural Modulus of Elasticity of Cement." Advanced Materials Research, 287-290, 990–993.